Green et al. *Light: Science & Applications* (2018)7:87
DOI 10.1038/s41377-018-0088-8

Official journal of the CIOMP 2047-7538
www.nature.com/lsa

ARTICLE Open Access

Doped, conductive SiO_2 nanoparticles for large microwave absorption

Michael Green[1], Zhanqiang Liu[2], Peng Xiang[3], Yan Liu[1,4], Minjie Zhou[1,5], Xinyu Tan[3], Fuqiang Huang[2], Lei Liu[6] and Xiaobo Chen[1]

Abstract

Although many materials have been studied for the purpose of microwave absorption, SiO_2 has never been reported as a good candidate. In this study, we present for the first time that doped, microwave conductive SiO_2 nanoparticles can possess an excellent microwave absorbing performance. A large microwave reflection loss (RL) of −55.09 dB can be obtained. The large microwave absorption originates mainly from electrical relaxation rather than the magnetic relaxation of the incoming microwave field. The electrical relaxation is attributed to a large electrical conductivity that is enabled by the incorporation of heterogeneous (N, C and Cl) atoms. The removal of the magnetic susceptibility only results in a negligible influence of the microwave absorption. In contrast, the removal of the heterogeneous atoms leads to a large decrease in the electrical conductivity and microwave absorption performance. Meanwhile, the microwave absorption characteristics can be largely adjusted with a change of the thickness, which provides large flexibility for various microwave absorption applications.

Introduction

The utility of microwave absorption is significant in many applications, such as wireless communications and anti-radar detection of aircraft[1–3]. For example, many materials have been developed to reduce the radar signature of aircraft, ships and tanks in military fields. Material examples include carboneous materials such as graphite[4], graphene[5], carbon nanotubes (CNTs)[6] and carbon fibers[7], conducting polymers[8], oxides such as Fe_2O_3[9], Fe_3O_4[10], MnO_2[11], ZnO[12], $BaFe_{12}O_{19}$[13], $BaTiO_3$[13], $SrFe_{12}O_{19}$[14], and carbides such as SiC[15] and SiCN[16]. Traditional mechanisms that are commonly believed to be responsible include dipole rotation and magnetic domain resonance due to the dielectric and magnetic losses inside the materials. For example, the microwave absorption of Ni-coated CNT/epoxy composites results from dielectric and magnetic losses, with the use of Ag nanowires shown to enhance the performance due to dielectric loss[3]. Conducting polymers such as polypyrrole, polyaniline and poly(3-octylthiophene) have been demonstrated to show good microwave absorption[8]. Suitable inclusion of Fe_2O_3 nanoparticles in polyaniline enhanced the microwave absorption properties due to simultaneous adjustment of dielectric loss and magnetic loss[9]. Hollow urchin-like MnO_2 nanostructures with tetragonal nanorod clusters showed better performance due to proper electromagnetic impedance matching[11]. $BaTiO_3$/polyaniline and $BaFe_{12}O_{19}$/polyaniline composites showed good compatible dielectric and magnetic properties for broadband microwave absorbing properties[13]. Recently, microwave absorption has been reported to be enhanced by defective or disorder structures such as oxygen vacancies, low crystallinity and use of a core/shell structure[1,2,17–19]. The dielectric properties of TiO_2[1,2,17,18], ZnO[2] and $BaTiO_3$[19] nanoparticles can be modified through the perturbation of their crystalline structure by hydrogenation treatment to enhance their microwave absorption performance. Gao and colleagues[20] have also found that the microwave

Correspondence: Xinyu Tan (tanxin@ctgu.edu.cn) or Fuqiang Huang (huangfq@mail.sic.ac.cn) or Xiaobo Chen (chenxiaobo@umkc.edu)
[1]Department of Chemistry, University of Missouri, Kansas City, MO 64110, USA
[2]State Key Laboratory of High Performance Ceramics and Superfine Microstructure, Shanghai Institute of Ceramics, Chinese Academy of Sciences, Shanghai 200050, China
Full list of author information is available at the end of the article.

dielectric properties of TiO_2 nanoparticles can be largely altered by introducing partial crystalline phases in such TiO_2 nanoparticles. Although these findings have provided a large pool of materials for microwave absorption applications, each material may have some advantages and disadvantages; therefore, it is highly desirable to discover new materials for microwave absorption. On the other hand, microwave absorption is also very useful for sample preparation with microwave irradiation in that rapid synthesis is enabled when compared to use of a traditional heating treatment[21,22].

Up to now, pure SiO_2 has not yet been reported to show a good microwave absorption performance, although an enhanced microwave performance for the composites of SiO_2/carbon[23], SiO_2/carbonyl iron[24] and SiO_2/iron[25] was obtained due to the combination of a proper electromagnetic impedance match[23–25]. This is understandable because in pure SiO_2 there is no good source for traditional microwave absorption mechanisms including dipole rotation and magnetic domain resonance due to dielectric and magnetic losses. The lack of origin for the creation of dipoles in pure SiO_2 nanoparticles is attributed to its symmetric structure where the dipoles are canceled in each tetrahedral unit of the SiO_2 lattice. Meanwhile, it is also unlikely that there will be magnetic domains to echo with the microwave electromagnetic field due to the lack of charge spin centers in pure SiO_2. Therefore, it is reasonable that pure SiO_2 will not be able to possess good mechanisms for efficient microwave absorption. To enable effective microwave absorption, we intentionally create dipoles in SiO_2 nanoparticles by introducing heterogeneous atoms such as C, N and Cl elements on the O sites inside the SiO_4 tetrahedra or simply linked onto the surface of the SiO_2 nanoparticles. Rotations of these induced dipoles can, therefore, echo with the incident microwave field to possess microwave absorption. Effective electrical loss can be achieved with such heterogeneous atoms by having higher electrical conductivity. Here, we report that the doped, microwave conductive SiO_2 nanoparticles can show excellent microwave absorption performance. In contrast, only poor microwave absorption performance is observed for the SiO_2 nanoparticles without the incorporation of the heterogeneous atoms, which lack dipole rotations and good electrical conductivity.

Materials and methods

Tetraethyl orthosilicate (TEOS), *N*,*N*′-dimethylformamide (DMF) and hydrazine monohydrochloride were purchased from Sigma-Aldrich and used as received. Typically, TEOS (2.2 mL) was slowly added to DMF (20.0 mL) under ambient conditions by vigorously stirring, producing a completely transparent solution. A desired amount of hydrazine monohydrochloride (2.74 g) was added and stirred for 5–10 min, which was then transferred into a Teflon-lined, stainless autoclave at a different temperature of 160 °C for 12 h, producing a light-yellow slurry, which was washed with anhydrous ethanol and dried at 100 °C. A light-yellow product was collected. For comparison, pure white SiO_2 nanoparticles were also prepared followed by calcination of the light-yellow sample at 600 °C in air for 2 h.

The crystal structure was examined using a Rigaku Miniflex X-ray diffractometer (XRD) with a Cu Kα ($\lambda = 0.15418$ nm) radiation source. The morphology and crystallinity were probed with transmission electron microscopy (TEM) and high-resolution TEM (HRTEM) on an FEI Tecnai F20 STEM under an electron accelerating voltage of 200 kV. The surface chemical properties were studied with a Kratos Axis 165 X-ray photoelectron spectrometer (XPS) equipped with an Al/Mg dual-anode X-ray source. All the XPS spectra were calibrated with the C 1s peak from the carbon tape to 284.6 eV. The energy-dispersive X-ray (EDX) spectrum was taken using a Tescan Vega 3 LMU scanning electron microscope equipped with a Bruker Quantax 6|10 EDX system. The Fourier transform infrared (FT-IR) spectra were collected using a Thermo-Nicolet iS10 FT-IR spectrometer equipped with an attenuated total reflectance unit. The complex permittivity and permeability were measured in the frequency range of 1.0–18.0 GHz using an HP8722ES network analyzer with ring-shape samples containing 60 wt% SiO_2 nanoparticles dispersed in paraffin wax. The ring had a thickness of 2.0 mm, an inner diameter of 3.0 mm and an outer diameter of 7.0 mm.

Results and discussion

The XRD pattern for the doped SiO_2 nanoparticles matched well with the standard card of SiO_2 (PDF#00-038-0360), as shown in Fig. 1b. The broadness of the broad peak at approximately 26.2° indicated that the nanoparticle size was small. The weak intensity suggested a poor crystallinity. From the TEM image in Fig. 1c, clearly, the nanoparticles were 4–8 nm in diameter (Fig. 1d). The HRTEM image in Fig. 1e exhibited clear lattice fringes with a plane distance of 0.245 nm corresponding to the (200) plane of monoclinic Moganite SiO_2. Meanwhile, some amorphous regions were also observed between the crystalline domains, suggesting the likely existence of an amorphous phase (as pointed out by the dashed lines). The small size and amorphous phase matched well with the broad diffraction peak from the XRD pattern. This coexistence of amorphous and crystalline domains in the doped SiO_2 nanoparticles was similar to that reported for TiO_2 nanoparticles showing enhanced microwave absorption;[1,2,20] this is because the amorphous phase may

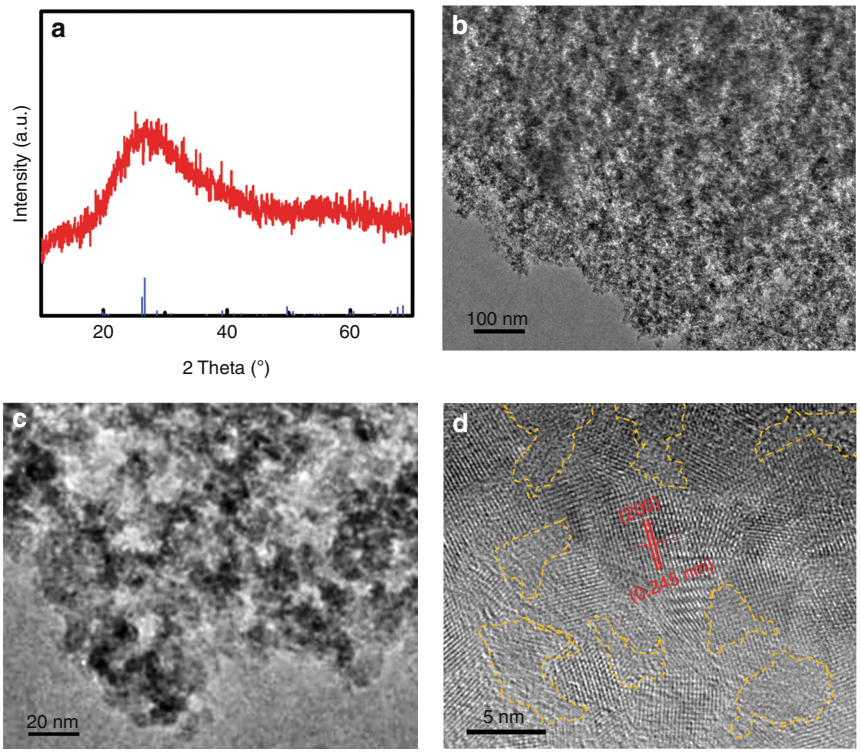

Fig. 1 Physical properties of SiO_2 nanoparticles. a XRD pattern, **b**, **c** TEM and **d** HRTEM images of SiO_2 nanoparticles. The panel (**a**) also shows the standard (PDF#00-038-0360). The yellow dashed lines in (**d**) point out the amorphous phases

create some interfacial dipole rotations along the interface with the crystalline phase and induce active microwave absorption[1,2,20]. The existence of Si, O, C, N and Cl elements were confirmed using results from XPS and EDX, as shown in Figure S1-S7. The surface of the doped SiO_2 nanoparticles was likely linked with the $-NH_2$ groups from the hydrazine hydrochloride and some adsorbed water and HCl molecules (Figure S8). The Si 2*p* spectrum (Figure S2) showed one peak with a binding energy centered approximately 103.2 eV, corresponding to the Si $2p_{3/2}$ in the SiO_2[26,27]. In the O 1s XPS spectrum shown in Figure S3, one peak was found to be centered approximately 532.6 eV, consistent with the binding energy of the O 1s signal from SiO_2[28,29]. The C 1s XPS spectrum (Figure S4) showed one minor peak centered approximately 284.6 eV, and one major peak approximately 286.4 eV. The former was likely from the adsorbed carbon during the XPS measurement, with the latter likely from the alkyl groups from the TEOS on the surface of the SiO_2 nanoparticles[30,31]. The N 1s spectrum in Figure S5 showed two peaks with a major contribution approximately 399.9 eV and a minor shoulder approximately 401.9 eV, likely from the N_2H_4 moiety and the conjugated NH_2 moiety attached to the HCl group from the hydrazine hydrochloride on the surface of the SiO_2 nanoparticles, respectively[32,33]. The Cl 2*p* XPS spectrum (Figure S6) displayed one higher peak approximately 197.6 eV and one lower peak near 199.3 eV, likely from the HCl coupled to the N_2H_4 moiety on the surface and the HCl coupled to the SiO_2 surface, respectively[34].

The variations of the microwave reflection loss (RL) with frequency (*f*) and thickness (*d*) were clearly displayed in a three-dimensional (3D) plot and two-dimensional (2D) contour, as shown in Fig. 2a, b. The 2D contour plot showed the projection of the 3D graph for the change of RL (indicated by the color ruler) on the frequency *f* and thickness *d* plane. The different colors indicated where (*f* and *d*) and which level of RL was achieved. Some representative RL curves were shown in Fig. 2c for varying *d* from 1.0 to 20.0 mm. The maximum microwave absorption frequency (f_{max}) was tunable with *d*. As *d* increased, f_{peak} shifted from higher frequency to lower frequency, as clearly seen in Fig. 2d. The relationship between f_{peak} and *d* was fitted very well with the formula $f/\mathrm{GHz} = 39.0/(d/\mathrm{mm})^{1.17}$ or $c/4f_{peak}\varepsilon'^{0.5} = \lambda/4\varepsilon'^{0.5}$, where *c* was the speed of light. Apparently, f_{peak} decreased reversibly with *d*. As *d* became bigger, f_{peak} decreased. The change in RL_{peak} with *d* (Fig. 2e) could be divided into two stages: a quick increase from −18.45 to −55.09 dB when *d*

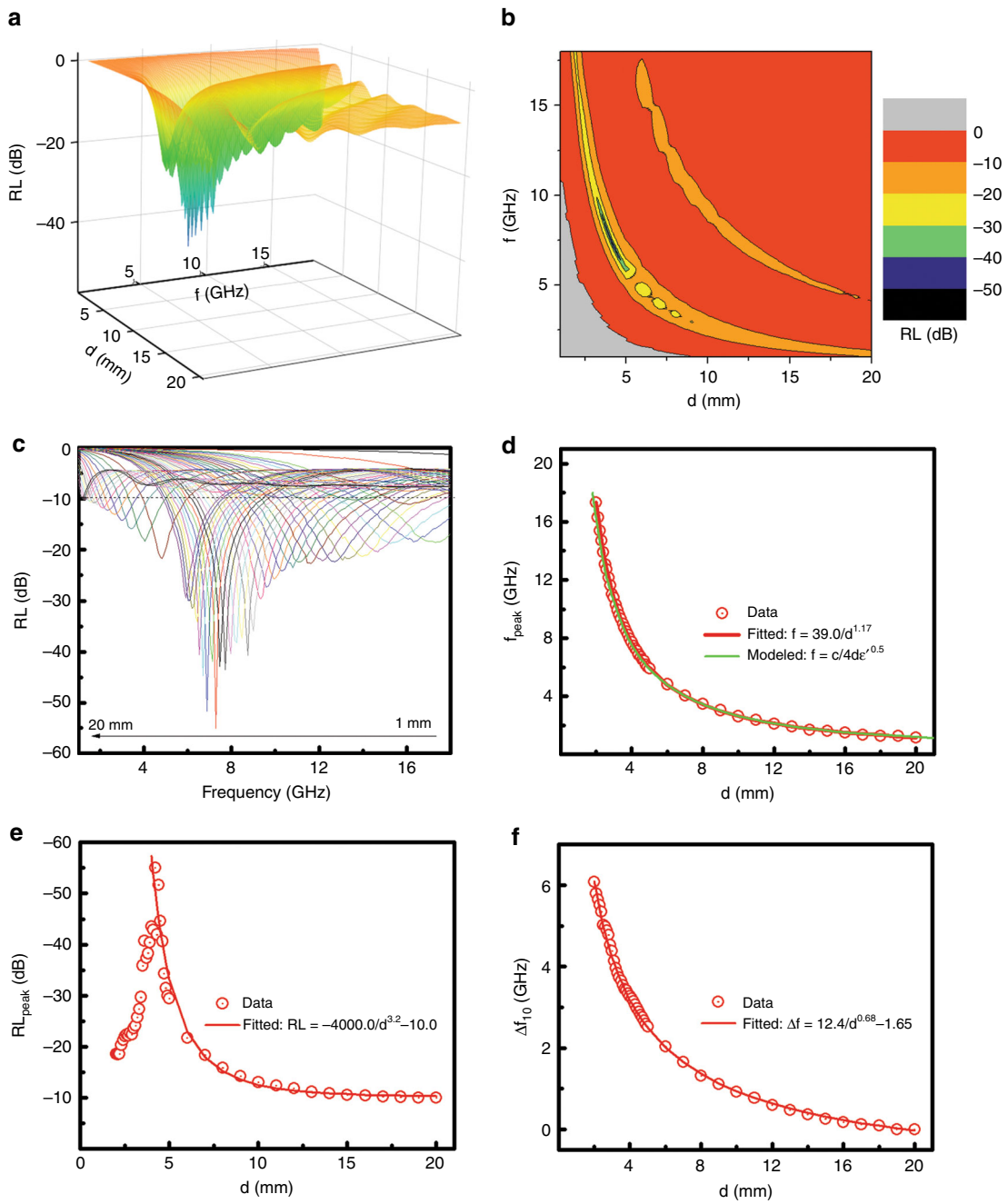

Fig. 2 Microwave absorption characteristics of SiO_2 nanoparticles. a The 3D plot and **b** 2D contour of the RL curves with *d* and *f*, **c** the RL curves, **b** the relationship for the **d** f_{peak}, **c**, **e** RL_{peak} and **d**, **f** Δf_{10} with *d* of the SiO_2 nanoparticles in the frequency range of 1.0–18.0 GHz

was changed from 2.0 to 4.2 mm, and a decay from −55.09 to −9.97 dB as *d* grew from 4.2 to 20.0 mm. The largest RL_{max} value (−55.09 dB) was observed when *d* was 4.2 mm. The change in Δf_{10} with *d* was shown in Fig. 2f and fitted very well with Δf_{10} /GHz = $12.4/(d/\text{mm})^{0.68} - 1.65$. As *d* became bigger, Δf_{10} almost decreased monotonically. This indicated that a thicker coating actually shielded a narrower region of microwave reflection frequency. It should be noted that the application of a thicker coating is very useful for the protection of important stationary objects on the ground from radar detection where a thin coating may not be able to shield such objects at a specific frequency, which is very important but frequently overlooked.

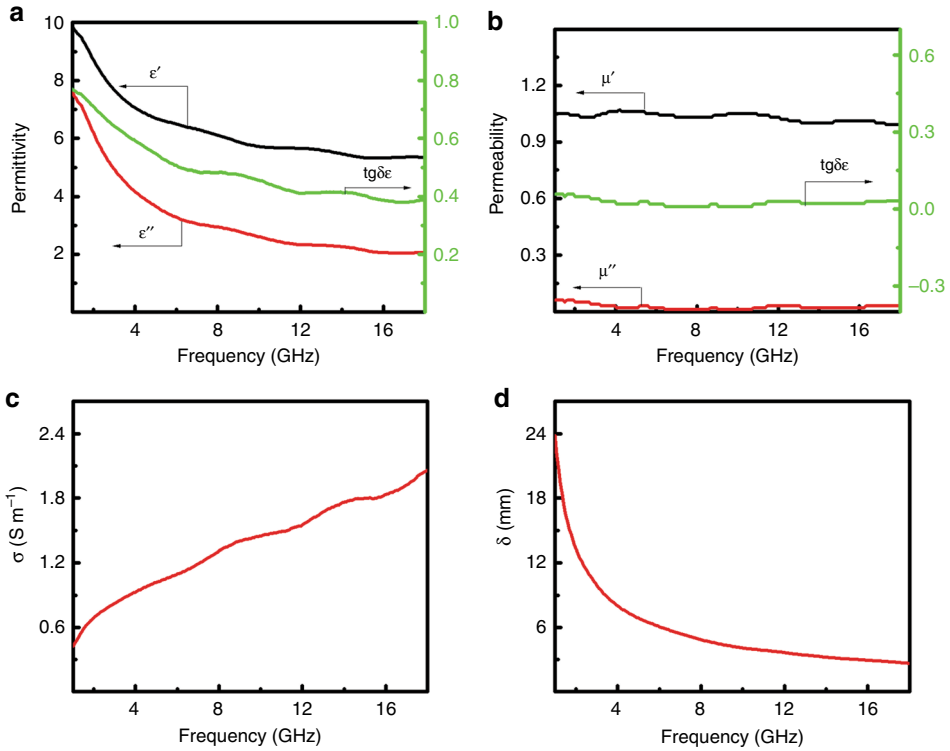

Fig. 3 The dielectric and magnetic properties of SiO_2 nanoparticles. a The complex permittivity (ε', ε'', $tg\delta_\varepsilon$), **b** complex permeability (μ', μ'', $tg\delta_\mu$), **c** electrical conductivity (σ) and **d** skin depth (δ) of the SiO_2 nanoparticles in the frequency range of 1.0–18.0 GHz

The microwave absorption properties are dependent on the dielectric and magnetic properties:

$$RL(dB) = 20log|(Z_{in} - Z_0)/(Z_{in} + Z_0)| \quad (1)$$

$$Z_{in} = Z_0(\mu_r/\varepsilon_r)^{1/2} tanh\left[j(2\pi fd/c)(\varepsilon_r\mu_r)^{1/2}\right] \quad (2)$$

where RL(dB) is the reflection loss in dB, Z_{in} is the input impedance of the absorber, Z_0 is the impedance of free space, μ_r is the relative complex permeability, ε_r is the relative complex permittivity, f is the frequency of the electromagnetic wave, d is the thickness of the absorber and c is the velocity of light[18]. As shown in Fig. 3a, when f increased from 1.0 to 18.0 GHz, ε' gradually decreased from 9.89 to 5.35, ε'' decreased slowly from 7.63 to 2.06 and $tg\delta_\varepsilon$ fell slowly from 0.77 to 0.39. Figure 3b showed that μ' decreased from 1.05 to 0.99, μ'' dropped from 0.06 to 0.03 and $tg\delta_\mu$ changed from 0.06 to 0.03 when f increased from 1.0 to 18.0 GHz. These results suggested that the doped SiO_2 nanoparticles had a smaller stored electrical and magnetic energy as the frequency of the incident electromagnetic field increased, indicating that some of the echoes of the electric field or dipoles to the oscillating field lagged behind and seemed consumed as the frequency increased.

The electrical conductivity (σ) shown in Fig. 3c was calculated with $\sigma\ (S\ m^{-1}) = 2\pi f\varepsilon_0\varepsilon''$, where ε_0 was the free space permittivity ($8.854 \times 10^{-12}\ F\ m^{-1}$), f was the frequency (Hz) and ε'' was the imaginary component of the permittivity[35]. The σ increased almost monotonically from 0.42 to 2.06 $S\ m^{-1}$ as f increased from 1.0 to 18.0 GHz. The large conductivity was suggested to be possibly related to the existence of the heterogeneous atoms (C, N, Cl) on the surface of the SiO_2 nanoparticles; for example, partial oxygen atoms were replaced with N atoms on the surface of the particles. The skin depth (δ) of the microwave irradiation in Fig. 3d was calculated with $(\delta/m) = (\pi f\mu_0\mu_r\sigma)^{-1/2}$, where μ_0 was the permeability of free space ($4\pi \times 10^{-7}\ H\ m^{-1}$), μ_r was the relative permeability and σ was the electrical conductivity ($S\ m^{-1}$)[33]. The δ decreased from 23.84 to 2.63 mm as f increased from 1.0 to 18.0 GHz.

To reveal the contribution of the permeability or the magnetic properties of the SiO_2 nanoparticles to the microwave absorption performance, we compared the microwave absorption results with and without the contribution of the magnetic components by assuming, for the latter case, a magnetic susceptibility parameter (χ_m) equal to zero, where $\mu_r = \mu/\mu_0 = (1 + \chi_m)\mu_0$. The evolution of the RL curves in Fig. 4a when d was changed from 1.0 to 20.0 mm indicated that as d increased, f_{peak} shifted to lower values. As shown in Fig. 4b, f_{peak} decreased as d increased, with their

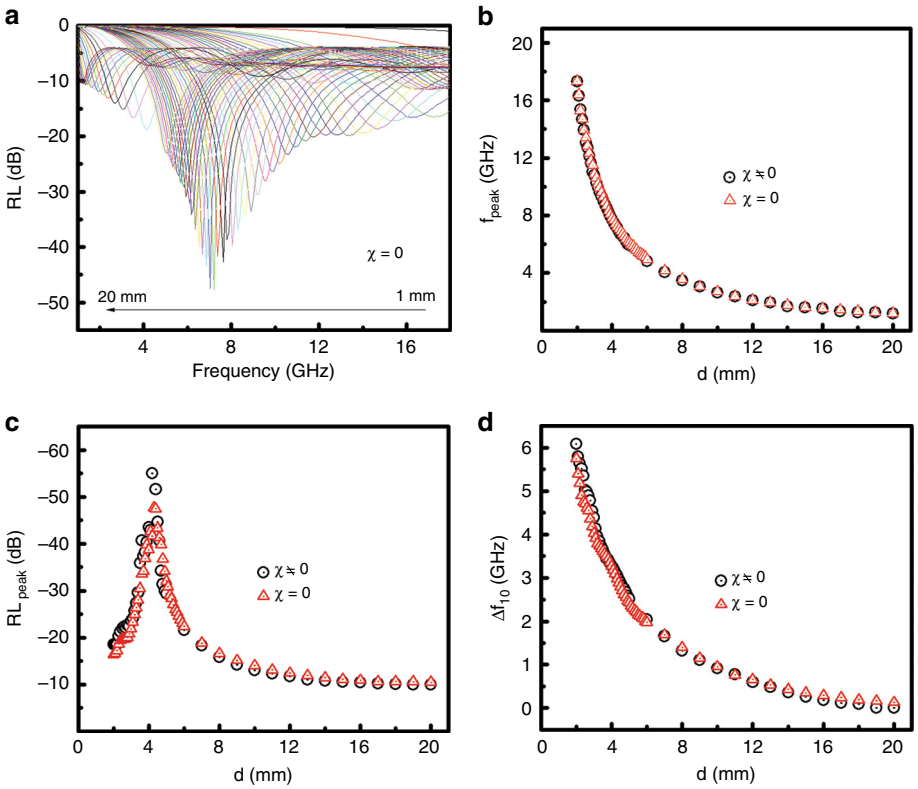

Fig. 4 Some microwave absorption characteristics of SiO_2 nanoparticles with/out magnetic contribution. a The RL curves when χ_m is zero, and a comparison of the relationships for the **b** f_{peak}, **c** RL_{peak} and **d** Δf_{10} with d, when χ_m is nonzero vs. zero for the SiO_2 nanoparticles in the frequency range of 1.0–18.0 GHz

relationships overlapping almost completely for nonzero and zero χ_m (see also Figure S9). RL_{peak} rapidly increased and then decayed with d, following the same trend for nonzero χ_m (Fig. 4c and Figure S10). Meanwhile, it was noticeable that the maximum RL_{peak} was smaller with a zero χ_m as d changed. Figure 4d compared the Δf_{10}–d relationships for nonzero and zero χ_m. The Δf_{10}–d trends overlapped very well (also see Figure S11) despite Δf_{10} being smaller at smaller d values and larger at larger d values for zero χ_m. This indicated that the influence of the none-zero χ_m for the SiO_2 nanoparticles was mainly reflected in the change of the Δf_{10} values. Overall, the none-zero χ_m increased the RL_{peak} and the Δf_{10} values possibly achieved at certain d values despite the overall impact being small. The small contribution of the magnetic property on the microwave absorption was related to the small μ" and $tg\delta_\mu$ values. The overall influence of the none-zero χ_m on the microwave absorption was clearly shown in Figure S12 as well.

Therefore, the large microwave absorption performance of the doped, conductive SiO_2 nanoparticles was most likely related to their dielectric properties, or the rotations of dipoles in the material as indicated by the large electrical conductivity in the microwave frequency range, as shown in Fig. 3c. In pure SiO_2 nanoparticles, no obvious origin was found for the creation of dipoles due to its symmetric structure where the dipoles likely canceled out each other in each tetrahedral unit of the SiO_2. However, in the doped SiO_2 nanoparticles, there were possible sources for the existence of dipoles due to the introduction of C, N and Cl elements as evidenced by the XPS results. Those atoms apparently broke down the symmetrical environment of the SiO_2 lattice, and created dipoles on the surface, causing the variation of the dielectric property across the nanoparticles and the increased conductivity. Under microwave irradiation, those dipoles might rotate and echo with the electromagnetic field to produce resonance, causing reflection loss, as schematically shown in Figure S13. Therefore, a large RL was observed in the case of a good match between the dielectric/magnetic properties with the incident microwave field.

To verify this conclusion, we measured the microwave absorption performance along with the dielectric and magnetic properties of those doped SiO_2 nanoparticles

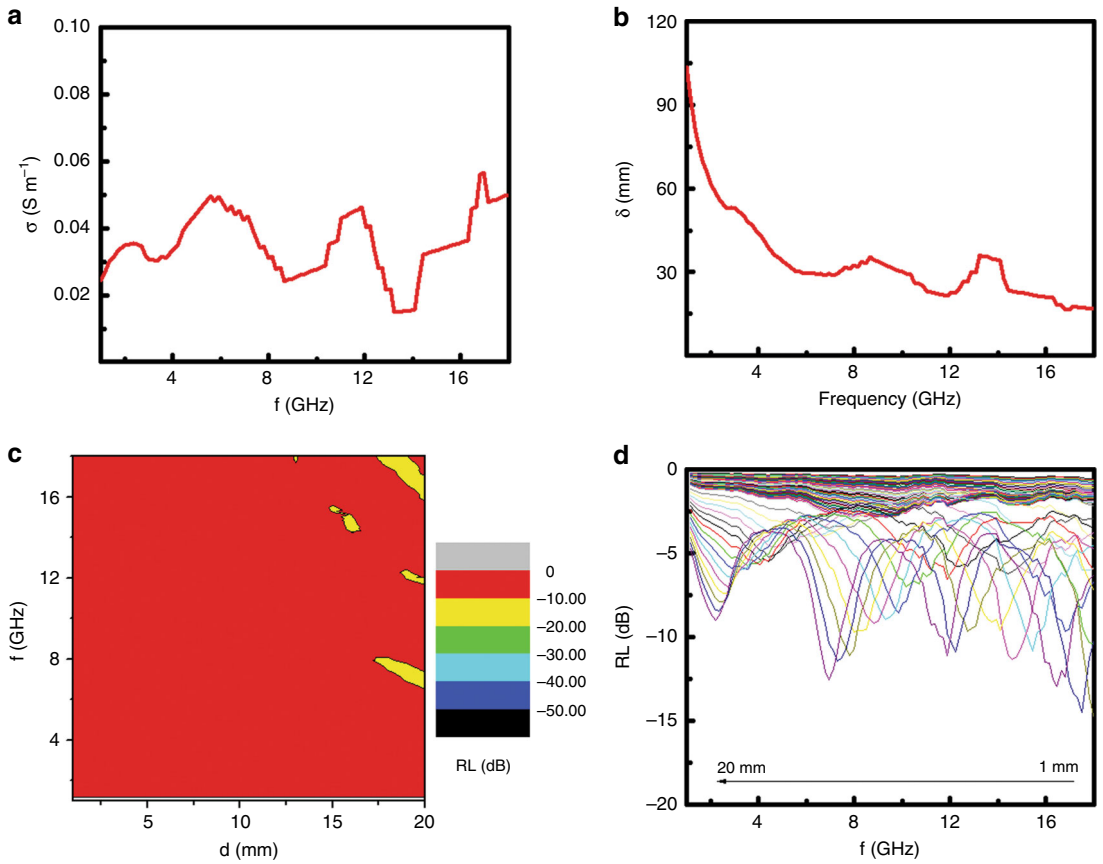

Fig. 5 Some dielectric and microwave absorption characteristics of calcinated, undoped SiO_2 nanoparticles. a The σ curve, **b** δ curve, **c** 2D contour plot for RL vs. *f* and *d* and **d** representative RL curves for the pure, poorly conductive SiO_2 nanoparticles obtained after calcination

after removal of the heterogeneous atoms by calcination at 600 °C for 2 h in air. The removal of those atoms was confirmed using XPS results (Figure S14-17) where no N and Cl atoms were observed, with the remaining C due to atmospheric deposition. Meanwhile, calcination at high temperature normally led to high crystallization and removal of the amorphous phase in the material. Compared to the doped SiO_2 nanoparticles, the calcinated, pure SiO_2 nanoparticles showed much smaller ε', ε" and $tg\delta_\varepsilon$ values (Figure S18), which matched well with the values in the literature[36], but showed similar μ', much larger μ" and $tg\delta_\mu$ values (Figure S19). As a result, these calcinated, pure SiO_2 nanoparticles only showed very small σ values (Fig. 5a) and large δ (Fig. 5b) values in the microwave region. The small σ values indicated that these SiO_2 nanoparticles were barely electrically conductive, with the large δ values suggesting that the microwave field was not efficiently decayed. Their poor microwave absorption performance was observed from the 2D contour plot of the RL over *f* and *d* in Fig. 5c and the RL plots in Fig. 5d, where the RL values were found to be less than −10 dB in most of the *d*–*f* regions. The poor microwave absorption performance of the calcinated SiO_2 nanoparticles further confirmed that the good microwave absorption performance of the doped SiO_2 nanoparticles was due to electrical relaxation, as the calcinated SiO_2 nanoparticles had much smaller electrical relaxation but much large magnetic relaxation. Meanwhile, the fact that the associated C, N and Cl atoms were removed from the SiO_2 nanoparticles after calcination also hinted that those heterogeneous atoms were likely linked onto the surface instead of being located in the bulk of the SiO_2 nanoparticles. Table S1 listed the microwave absorption performance of various materials that have been studied. As seen, doped, microwave conductive SiO_2 showed an impressive microwave absorption performance. Therefore, such materials are a promising candidate for microwave absorption. The importance of electrical relaxation on the microwave absorption is consistent with the conclusion made in the studies by Mao and colleagues[37–43]. Furthermore, such materials can be shown to be very useful in self-powered electromagnetic energy conversion and microwave attenuation, as demonstrated by

Mao and colleagues[40,41], which we plan to build in our future work.

Conclusions

In summary, in this study we have shown that doped, microwave conductive SiO_2 nanoparticles possess an exciting microwave absorbing performance, benefiting from the good electrical conductivity that is induced by the incorporation of heterogeneous (N, C and Cl) atoms on the surface of the SiO_2 nanoparticles. A large RL value of −55.09 dB can be obtained. The microwave absorption is mainly related to the dielectric loss resulting from the good electrical conductivity, while the small contribution of the magnetic property may be directly related to the small μ" and $tg\delta_\mu$. In contrast, calcinated, pure SiO_2 nanoparticles show a poor electrical conductivity and microwave absorption performance even with a larger magnetic response. In addition, microwave absorption characteristics such as f_{peak}, RL_{peak} and Δf_{10} can be largely adjusted with the thickness of the doped, conductive SiO_2 nanoparticles, which provides large flexibility for their microwave application towards various purposes.

Acknowledgements

X.C. appreciates the support from the U.S. National Science Foundation (DMR-1609061) and the College of Arts and Sciences, University of Missouri–Kansas City. L.L. acknowledges the support from the National Science Fund for Distinguished Young Scholars of China (No. 61525404). M.Z. acknowledges the support from the National Natural Science Foundation of China (Grant No. 51372080). X.T. is thankful for the support from the National Natural Science Foundation of China (U1765105). F.H. appreciates the support from the National Key Research and Development Program of China (2016YFB0901600).

Author details

[1]Department of Chemistry, University of Missouri, Kansas City, MO 64110, USA. [2]State Key Laboratory of High Performance Ceramics and Superfine Microstructure, Shanghai Institute of Ceramics, Chinese Academy of Sciences, Shanghai 200050, China. [3]College of Materials and Chemical Engineering, Hubei Provincial Collaborative Innovation Center for New Energy Microgrid, China Three Gorges University, Yichang 443002, China. [4]College of Environment, Sichuan Agricultural University, Chengdu, Sichuan 611130, China. [5]School of Chemistry and Chemical Engineering, Hunan Institute of Science and Technology, Yueyang 414000, China. [6]State Key Laboratory of Luminescence and Applications, Changchun Institute of Optics, Fine Mechanics and Physics, Chinese Academy of Sciences, Changchun 130033, China

Conflict of interest

The authors declare that they have no conflict of interest.

Supplementary information is available for this paper at https://doi.org/10.1038/s41377-018-0088-8.

Received: 25 April 2018 Revised: 16 October 2018 Accepted: 17 October 2018
Published online: 14 November 2018

References

1. Xia, T., Zhang, C., Oyler, N. A. & Chen, X. B. Hydrogenated TiO_2 nanocrystals: a novel microwave absorbing material. *Adv. Mater.* **25**, 6905–6910 (2013).
2. Xia, T. et al. Strong microwave absorption of hydrogenated wide bandgap semiconductor nanoparticles. *ACS Appl. Mater. Interfaces* **7**, 10407–10413 (2015).
3. Zhao, D. L., Li, X. & Shen, Z. M. Microwave absorbing property and complex permittivity and permeability of epoxy composites containing Ni-coated and Ag filled carbon nanotubes. *Compos Sci. Technol.* **68**, 2902–2908 (2008).
4. Fan, Y. Z., Yang, H. B., Li, M. H. & Zou, G. T. Evaluation of the microwave absorption property of flake graphite. *Mater. Chem. Phys.* **115**, 696–698 (2009).
5. Zhang, Y. et al. Broadband and tunable high-performance microwave absorption of an ultralight and highly compressible graphene foam. *Adv. Mater.* **27**, 2049–2053 (2015).
6. Fan, Z. J., Luo, G. H., Zhang, Z. F., Zhou, L. & Wei, F. Electromagnetic and microwave absorbing properties of multi-walled carbon nanotubes/polymer composites. *Mater. Sci. Eng. B* **132**, 85–89 (2006).
7. Li, G., Xie, T. S., Yang, S. L., Jin, J. H. & Jiang, J. M. Microwave absorption enhancement of porous carbon fibers compared with carbon nanofibers. *J. Phys. Chem. C* **116**, 9196–9201 (2012).
8. Olmedo, L., Hourquebie, P. & Jousse, F. Microwave absorbing materials based on conducting polymers. *Adv. Mater.* **5**, 373–377 (1993).
9. Wang, Z. Z., Bi, H., Liu, J., Sun, T. & Wu, X. L. Magnetic and microwave absorbing properties of polyaniline/γ-Fe_2O_3 nanocomposite. *J. Magn. Magn. Mater.* **320**, 2132–2139 (2008).
10. Jia, K., Zhao, R., Zhong, J. C. & Liu, X. B. Preparation and microwave absorption properties of loose nanoscale Fe_3O_4 spheres. *J. Magn. Magn. Mater.* **322**, 2167–2171 (2010).
11. Zhou, M. et al. Morphology-controlled synthesis and novel microwave absorption properties of hollow urchinlike α-MnO_2 nanostructures. *J. Phys. Chem. C* **115**, 1398–1402 (2011).
12. Li, H. F. et al. Directed growth and microwave absorption property of crossed ZnO netlike micro-/nanostructures. *J. Phys. Chem. C* **114**, 10088–10091 (2010).
13. Yang, C. C., Gung, Y. J., Hung, W. C., Ting, T. H. & Wu, K. H. Infrared and microwave absorbing properties of $BaTiO_3$/polyaniline and $BaFe_{12}O_{19}$/polyaniline composites. *Compos Sci. Technol.* **70**, 466–471 (2010).
14. Kuruva, P., Matli, P. R., Mohammad, B., Reddigari, S. & Katlakunta, S. Effect of Ni–Zr codoping on dielectric and magnetic properties of $SrFe_{12}O_{19}$ via sol–gel route. *J. Magn. Magn. Mater.* **382**, 172–178 (2015).
15. Kuang, J. L., Jiang, P., Ran, F. Y. & Cao, W. B. Conductivity-dependent dielectric properties and microwave absorption of Al-doped SiC whiskers. *J. Alloy. Compd.* **687**, 227–231 (2016).
16. Li, Q. et al. Dielectric and microwave absorption properties of polymer derived SiCN ceramics annealed in N_2 atmosphere. *J. Eur. Ceram. Soc.* **34**, 589–598 (2014).
17. Xia, T., Zhang, C., Oyler, N. A. & Chen, X. B. Enhancing microwave absorption of TiO_2 nanocrystals via hydrogenation. *J. Mater. Res.* **29**, 2198–2210 (2014).
18. Tian, L. H. et al. Broad range energy absorption enabled by hydrogenated TiO_2 nanosheets: from optical to infrared and microwave. *J. Mater. Chem. C* **5**, 4645–4653 (2017).
19. Tian, L. H. et al. Effect of hydrogenation on the microwave absorption properties of $BaTiO_3$ nanoparticles. *J. Mater. Chem. A* **3**, 12550–12556 (2015).
20. Dong, J. Y. et al. Partially crystallized TiO_2 for microwave absorption. *J. Mater. Chem. A* **3**, 5285–5288 (2015).
21. Guo, Y. F. et al. A rapid microwave-assisted thermolysis route to highly crystalline carbon nitrides for efficient hydrogen generation. *Angew. Chem. Int Ed.* **55**, 14693–14697 (2016).
22. Xu, W. T. et al. A general and rapid approach to crystalline metal sulfide nanoparticle synthesis for photocatalytic H_2 generation. *J. Mater. Chem. A* **5**, 21669–21673 (2017).
23. Chen, L. Y., Duan, Y. P., Liu, L. D., Guo, J. B. & Liu, S. H. Influence of SiO_2 fillers on microwave absorption properties of carbonyl iron/carbon black double-layer coatings. *Mater. Des.* **32**, 570–574 (2011).
24. Qing, Y. C., Zhou, W. C., Jia, S., Luo, F. & Zhu, D. M. Microwave electromagnetic property of SiO_2-coated carbonyl iron particles with higher oxidation resistance. *Phys. B* **406**, 777–780 (2011).
25. Yan, L. et al. Enhanced microwave absorption of Fe nanoflakes after coating with SiO_2 nanoshell. *Nanotechnology* **21**, 095708 (2010).
26. Ingo, G. M., Dirè, S. & Babonneau, F. XPS studies of SiO_2-TiO_2 powders prepared by sol-gel process. *Appl. Surf. Sci.* **70-71**, 230–234 (1993).
27. Koshizaki, N., Umehara, H. & Oyama, T. XPS characterization and optical properties of Si/SiO_2, Si/Al_2O_3 and Si/MgO co-sputtered films. *Thin Solid Films* **325**, 130–136 (1998).

28. Miller, M. L. & Linton, R. W. X-ray photoelectron spectroscopy of thermally treated silica (SiO_2) surfaces. *Anal. Chem.* **57**, 2314–2319 (1985).
29. Seyama, H. & Soma, M. Bonding-state characterization of the constitutent elements of silicate minerals by X-ray photoelectron spectroscopy. *J. Chem. Soc. Faraday Trans. 1* **81**, 485–495 (1985).
30. Clark, D. T. & Thomas, H. R. Applications of ESCA to polymer chemistry. XVII. Systematic investigation of the core levels of simple homopolymers. *J. Polym. Sci. Polym. Chem. Ed.* **16**, 791–820 (1978).
31. Briggs, D. & Beamson, G. Primary and secondary oxygen-induced C1s binding energy shifts in x-ray photoelectron spectroscopy of polymers. *Anal. Chem.* **64**, 1729–1736 (1992).
32. Srinivasan, R. & Walton, R. A. X-ray photoelectron spectra of inorganic molecules.: XX. Observations concerning the sulfur 2p binding energies in metal complexes of thiourea. *Inorg. Chim. Acta* **25**, l85–l86 (1977).
33. Biner, H. & Sellman, D. Z. X-ray photoelectron studies of pentacarbonyl chromium and tungsten complexes with nitrogen ligands. *Naturforsch. B* **33**, 173–179 (1978).
34. Andersson, M., Blomquist, J., Folkesson, B., Larsson, R. & Sundberg, P. Esca, mössbauer and infrared spectroscopic investigations of a series of tin complexes. *J. Electron Spectrosc. Relat. Phenom.* **40**, 385–396 (1986).
35. Micheli, D. *Radar Absorbing Materials and Microwave Shielding Structures Design: By Using Multilayer Composite Materials, Nanomaterials and Evolutionary Computation* (LAP LAMBERT Academic Publishing, Berlin, 2011).
36. Cao, M. S. et al. Microwave absorption properties and mechanism of cagelike ZnO/SiO_2 nanocomposites. *Appl. Phys. Lett.* **91**, 203110 (2007).
37. Wang, X. X., Ma, T., Shu, J. C. & Cao, M. S. Confinedly tailoring Fe_3O_4 clusters-NG to tune electromagnetic parameters and microwave absorption with broadened bandwidth. *Chem. Eng. J.* **332**, 321–330 (2018).
38. Liu, J. et al. Electromagnetic property and tunable microwave absorption of 3D nets from nickel chains at elevated temperature. *ACS Appl. Mater. Interfaces* **8**, 22615–22622 (2016).
39. Liu, J. et al. Enhanced permittivity and multi-region microwave absorption of nanoneedle-like ZnO in the X-band at elevated temperature. *J. Mater. Chem. C* **3**, 4670–4677 (2015).
40. Cao, M. S. et al. Thermally driven transport and relaxation switching self-powered electromagnetic energy conversion. *Small* **14**, 1800987 (2018).
41. Wen, B. et al. Temperature dependent microwave attenuation behavior for carbon-nanotube/silica composites. *Carbon* **65**, 124–139 (2013).
42. Wen, B. et al. Reduced graphene oxides: light-weight and high-efficiency electromagnetic interference shielding at elevated temperatures. *Adv. Mater.* **26**, 3484–3489 (2014).
43. Cao, M. S., Song, W. L., Hou, Z. L., Wen, B. & Yuan, J. The effects of temperature and frequency on the dielectric properties, electromagnetic interference shielding and microwave-absorption of short carbon fiber/silica composites. *Carbon* **48**, 788–796 (2010).